DETERMINATION OF RELATIVE SPIN CONCENTRATION IN SOME HIGH-SPIN FERRIC PROTEINS USING E/D-DISTRIBUTION IN ELECTRON PARAMAGNETIC RESONANCE SIMULATIONS

AN-SUEI YANG AND BETTY JEAN GAFFNEY
Department of Chemistry, The Johns Hopkins University, Baltimore, Maryland 21218

ABSTRACT Lineshape simulations are presented for the multiple, overlapping X-band electron paramagnetic resonance (EPR) spectra in two non-heme, high-spin iron proteins: phenylalanine hydroxylase (PAH) and diferric transferrin. The aim of the calculations is to determine the fraction of iron contributing to each of the sites visible by EPR. The simulations are limited to the experimentally accessible transitions occurring at g-values >1.7. In both PAH and transferrin, at least one of the iron sites is characterized by the ratio of zero-field splitting parameters, E/D, near 1/3 and a broad, asymmetric lineshape. A distribution in E/D-values is used in the simulations to account for this breadth and asymmetry. To test the E/D-distribution model, experimental X-band spectra of diferric transferrin at several salt concentrations are fit by simulation. In this test, first the low-field features arising from transitions between the lowest Kramers doublet levels are simulated using E/D-distributions for two sites. Second, parameters that provide a good fit for the lowest doublet transitions are shown also to fit the resonance near an effective g-value of 4.3 from the middle Kramers doublet transition. When applied to spectra of PAH in the resting state, the E/D-distribution approach accounts for the intensity of one of the two major species of iron. The other species is characterized by $E/D = 0.032$, and the spectrum of this portion of the resting enzyme may be simulated using a frequency-swept Gaussian lineshape. Spectra for the enzyme in an inhibitor-saturated state are also simulated. The simulations are consistent with previous biochemical studies that indicate that only the $E/D = 0.032$ form of iron participates in catalysis.

INTRODUCTION

It was shown recently that the non-heme iron enzyme, phenylalanine hydroxylase (PAH), has a high-spin iron ($S = 5/2$) electron paramagnetic resonance (EPR) signal composed of at least two components when the enzyme is in the resting state (1). PAH is a tetramer of four identical subunits with one iron per subunit. The specific activity of the enzyme is variable from preparation to preparation and the relative proportions of the two components in the EPR spectrum vary in a manner suggesting a correlation with specific activity. However, for field-swept EPR at constant frequency, double integration is completely unacceptable as a means of estimating spin concentration if the anisotropy in the effective g-tensor is large, as it may be for high-spin iron. Instead, spectral simulation is required to analyze the relationship between EPR and enzyme activity in PAH. The component in the experimental PAH EPR spectrum that appears on biochemical grounds (2) to correspond to active enzyme has prominent features at effective g-values, g', of 6.7 and 5.3.[1] This portion of the spectrum can be simulated using a lineshape that is Gaussian in the frequency domain. The other component has a prominent signal at $g' = 4.3$, presumably from the middle Kramers doublet transition of a high-spin iron species with almost maximum rhombicity. The lineshape of this component has very broad and asymmetric tails that are not easily simulated. There is a third type of spectrum that can be obtained with PAH, that of the enzyme–substrate complex. This complex does not turn over in the absence of cofactor and thus is a stable entity for EPR studies. The inhibitor, 4-fluorophenylalanine forms a complex with the enzyme that has an EPR spectrum similar to that of the enzyme–substrate complex. In this complex, both types of iron have nearly rhombic symmetry with peaks in the EPR centered around $g' = 4.3$ and again, broad tails from at least one component are observed. The EPR spectrum of ferric transferrin has similar broad tails around sharp intensity at $g' = 4.3$, and the details of the transferrin lineshape depend on salt concentration (3, 4).

Correspondence should be addressed to B. J. Gaffney.

[1]Effective g-values, g', are defined by the resonance condition: $g' = h\nu_0/\mu_B B_r$, where B_r is the resonant field and ν_0 the applied microwave frequency.

This paper uses transferrin as a model to develop a simulation that adequately accounts for the salt-dependence of the broad portions of the EPR spectra of this protein and then applies the approach to the spectra of PAH in the resting and inhibitor-bound states. It is shown that simulation gives fractional occupation of the two major sites in PAH that agrees well with fractional enzyme activity.

The spin Hamiltonian for high-spin iron is given by

$$H = g\mu_B B_0 \cdot S + D[S_z^2 - \tfrac{1}{3}S(S+1)] + E(S_x^2 - S_y^2) + \text{other terms.} \quad (1)$$

The expressions included in "other terms" depend on the choice of states as the basis set for the Hamiltonian. For a pure high-spin state ($L = 0$, $S = 5/2$), the spin Hamiltonian simplifies to only the first three terms. For mixture of the $^6A_1$ ground state with excited $^4T_1$ and $^2T_2$ states, 24 states are included in the complete basis set although approximations using fewer states are often adequate in simulations (5–7). The simulations presented here use a Hamiltonian for a pure high-spin state (i.e., only the first three terms in Eq. 1). The experimental justification for this choice is based on estimates of the magnitude of the zero-field splitting parameter, D, for PAH and transferrin. The sharp components of the spectra from both of these proteins have $D \leq 1$ cm^{-1}. The assumption is made that the components of these samples that give broad EPR signals also have $D \leq 1$ cm^{-1}. For these values of D, the samples are expected to be almost pure high spin. The simulations are also limited to regions corresponding to g'-values >1.7 because the limited solubility of the proteins precludes observation of signals of low intensity at smaller g'-values. Previous simulations based on the Hamiltonian Eq. 1 have been of two types: those with the zero-field splitting or Zeeman terms dominant (8–10) and those in which the two parts have comparable magnitude (11–17). The first case can be treated by perturbation theory. Because of the small D values of PAH and transferrin, the latter case applies at X-band or greater frequency and the secular determinant must be diagonalized. In earlier papers using this approach (11, 12), plots in reduced coordinates are given of resonance positions as a function of zero-field splittings for alignments of the field with the molecular principal axes. When $D/h\nu$ is small, points where the angular variation of the resonance position changes sign ($dB_r/d(\theta,\phi) = 0$) occur at positions other than along the principal axis directions so that extra powder lines appear. Also, $B_r/h\nu$ vs. $D/h\nu$ plots may be inadequate for predicting the positions of maxima and minima in actual lineshapes because they cannot account for anisotropic transition probabilities. Therefore, it is necessary to perform a complete lineshape simulation to account for experimental spectra (13–17). In addition, recent advances in understanding the implications of field-swept EPR (18–21) and numerous new experimental EPR spectra of high-spin ferric proteins, of which PAH is one example, provide a renewed need to compare simulated EPR spectra with experimental ones. For these reasons, an Appendix is provided that emphasizes the variation with D of the low-field region of simulated EPR spectra for $S = 5/2$ at X-band.

In some of the simulations presented here, a Gaussian distribution of E/D-values is used in simulating EPR features with broad tails. Distribution in E/D reflects heterogeneity in the geometry of iron ligands in the frozen samples used for EPR. To approximate the contribution of this heterogeneity to the lineshape, a series of spectra centered about a particular E/D-value is weighted by a Gaussian intensity factor and the series is summed numerically. This treatment of lineshapes is similar to the one used by Brill et al. (5, 22) to account for the excess breadth of lines in frozen solution, compared to single crystals, for high-spin ferrihemoglobin. For ferrihemoglobin samples, it was appropriate also to include a quartet of $^4T_1$ states mixing with the ground $^6A_1$ state, and a distribution in the extent of mixing, in simulations. Other authors (23–25) have used lineshapes based on distributions in either of the crystal field parameters, D or E, by deriving the width of these parameters, ΔD and ΔE, from the spin Hamiltonian by a first-order perturbation treatment.

SIMULATION PROCEDURES

The field-swept absorption spectrum of a powder distribution of spins is simulated by numerical integration as indicated in Eq. 2. In Eq. 2, $M(n)$ is the Boltzmann weighting factor, $P_{ij}(\theta,\phi)$ is the transition probability

$$S(B) = \sum_{n=1}^{N} \cdot M(n) \int_0^{\pi/2} \int_0^{\pi/2} P_{ij}(\theta,\phi)\, \delta B_r/\delta\nu\, Y(B) \sin\theta \, d\theta \, d\phi, \quad (2)$$

defined below by Eq. 3 and $Y(B)$ is a lineshape function that will be described in the next section. The partial derivative, $\partial B_r/\partial_\nu$, results when an expression for a frequency-swept spectrum is replaced by one for field-swept spectroscopy (18). The rotation axes shown in Fig. 1 define the angles θ and ϕ in Eq. 2 and χ (see Eq. 3 below). The direction cosines, ℓ, m, and n, of the microwave field, B_1, in this system are the same as those given by Van Veen (19; Eq. A7). For high-spin iron ($S = 5/2$), there are 15 transitions possible ($N = 15$) between i and j levels ($i, j = 1$–6), although only a few of these contribute significantly to X-band spectra at fields <4 kG. The relative transition probability of the ith to jth state (P_{ij}) is obtained by the integration indicated in Eq. 3 of the transition moment over χ, the angle between the microwave field and the vector **OP** (Fig. 1):

$$P_{ij}(\theta,\phi) = \frac{2\pi}{h^2}\mu_B{}^2 B_1^2 g^2 \int_0^{\pi} |\ell \langle i|S_x|j\rangle + m\langle i|S_y|j\rangle + n\langle i|S_z|j\rangle|^2 d\chi. \quad (3)$$

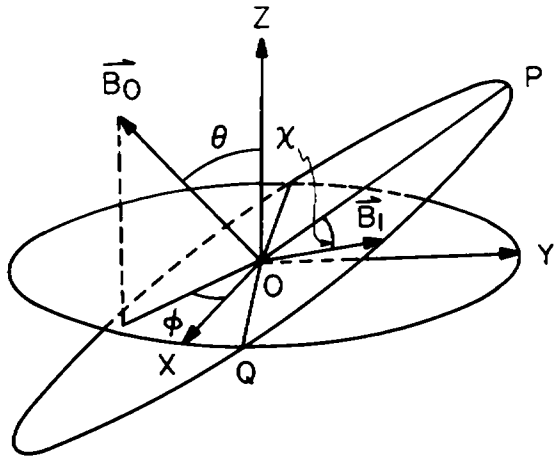

FIGURE 1 The molecular and laboratory axes and angles relating them are given for the EPR simulations. *OX*, *OY*, *OZ* are the molecular principal axes, B_0 is the external magnetic field, B_1 is the microwave field, and θ and ϕ are the polar angles projecting the laboratory coordinates onto the molecular ones. B_1 is perpendicular to B_0. *OP* is perpendicular to *OQ*. χ is the angle between B_1 and *OP*.

In Eq. 3, wave functions are used for which the coefficients, a_{ji}, are the components of the ith eigenvector of the 6 × 6 secular determinant given in Appendix Table III. This determinant also provides the effective g-value for each value of θ and ϕ.

The outline of a simulation is (*a*) assign ν_0, E/D, and D and divide θ and ϕ into increments, (*b*) use Table III to solve for g' at each value of θ and ϕ, (*c*) obtain the corresponding transition probability from Eq. 3, (*d*) apply a lineshape scaled by P_{ij} at each value of g', extending until the amplitude has dropped to 0.05 of the value at g', (*e*) perform the integration over θ and ϕ, and (*f*) repeat this calculation over a range of E/D-values if required. This procedure gives some mosaic ripple in the computed spectra which can be reduced by lowering the angular mesh from 5° to 2°. The process of fitting simulation to experiment with calculations that include E/D-distribution is simplified by storing spectra simulated at various E/D-values, weighting appropriate spectra by a Gaussian distribution, and summing these spectra for a particular application. A further simplification can be used when simulations are done for the lowest Kramers doublet transition for cases in which E/D is near ⅓. Here the lowest-field maximum is at the position of the y-principal value of the g'-tensor and the low-field feature can be fit well using a single orientation of the external field, B_0, along the y-principal axis. Matrix diagonalization in step *b* above was performed using International Mathematical and Statistical Library subroutines. Also in step *b*, an iterative bisection method was used to determine B_r. As an example of a calculation without E/D distribution, calculation of the lowest Kramers doublet transition (component II) in Fig. 8 required summing 342 individual derivative curves, and the calculation required ~3 min of cpu using a VAX 11/785 system. When distribution in E/D is included, the simulation time is lengthened.

LINESHAPES

Two types of considerations have contributed to an accurate analysis of the lineshapes for the ferric proteins considered here. The first involves the consequences of transforming expressions that describe a frequency-swept, constant-field spectrum, to appropriate expressions for the usual experimental situation of field-swept, constant-frequency spectroscopy. The second set of considerations concerns broadening of the lineshapes as a result of distributions in the parameters in the spin Hamiltonian Eq. 1. These considerations are discussed separately below.

The consequences of rewriting expressions for a frequency-swept EPR spectrum as expressions for the field-swept equivalent were discussed first by Aasa and Vänngard (18) and then, in depth, by Van Veen (19), Pilbrow et al. (20), and Pilbrow (21). These consequences are particularly important in simulating spectra that extend over a large range of g'-values and they may be a source of lineshape asymmetry. In summary, the above authors note that $Y[(\nu - \nu_0)/\Delta\nu]$ may be replaced by $1/g'\,Y[(B - B_r)/\Delta B]$ in defining a field-swept spectrum under the special conditions that P_{ij} and $\Delta\nu$ are not functions of field. Using the resonance condition given in footnote 1 to express the linewidth, ΔB, in terms of the proper linewidth, $\Delta\nu$, Eq. 4 is obtained

$$\Delta\nu(\text{MHz}) \times 0.714/g' = \Delta B(\text{G}). \tag{4}$$

Eq. 4 assumes a linear relationship between ν_0 and B_r within the region encompassed by a lineshape of width ΔB. In the simulations presented below, the individual linewidths, ΔB, are chosen to be narrow enough that Eq. 4 is a good approximation. Derivative lineshape expressions for field-swept spectra were given by Pilbrow (21) and are presented in equivalent form below in Eq. 5 for Lorentzian and Eq. 6 for Gaussian shapes.

$$\frac{dY_L}{dB} = -\frac{g'\mu_B}{h} \cdot \frac{2}{\pi\Delta\nu^2} \cdot \frac{B - B_r}{\Delta B} \cdot \left[\frac{1}{\left(1 + \frac{B - B_r}{\Delta B}\right)^2}\right]^2 \tag{5}$$

$$\frac{dY_G}{dB} = -\frac{g'\mu_B}{h} \cdot \frac{2(\ln 2)^{3/2}}{\sqrt{\pi}\,\Delta\nu} \cdot \frac{B - B_r}{\Delta B} \cdot e^{-\ln 2(B - B_r/\Delta B)^2}. \tag{6}$$

With the lineshapes written in this form, ΔB is the half-width at half-height of the absorption spectrum. Note that Eq. 4 means that, while $\Delta\nu$ is a constant for all regions of a powder spectrum with large g'-factor anisotropy, ΔB varies as $1/g'$ throughout the spectral region. In cases where the anisotropy in g' is small (e.g., the middle Kramers doublet transition when $g' \simeq 4.3$), a field-swept lineshape may be used as an approximation. The term $(g'\mu_B/h)$ in Eqs. 5 and 6 results simply from taking the derivative of the expressions for the absorption lineshapes (21).

The field-positions of the maxima in the EPR of $S = 5/2$ iron vary with E/D (see Figs. 11 and 12). The variation is nonlinear in E/D and differs from the dependence of field position on $1/g'$. For these reasons, simulations that invoke a distribution of E/D-values will not be equivalent to ones based on a simple Gaussian lineshape of large width or on a distribution of g'-values. Inhomogeneous broadening due to a distribution in either E/D (5, 23) or g' (26, 27) results in lineshapes that are broadened to the high-field side for a particular molecular orientation. For the simulations discussed here, distribution in E/D is introduced by summing a set of calculations in which the ratio (R) of E/D is varied in steps and the amplitude, $A(R)$, of each contribution follows a Gaussian distribution of width ΔR about a value, R_0 (Eq. 7). The individual calculations at each E/D-value are based on a field-swept Lorentzian shape of width ΔL and are also weighted by the transition probability for that E/D.

$$A(R) = \frac{1}{g'} P_{ij}(\theta, \phi, R)\, e^{-1/2(R-R_0/\Delta R)^2}, \qquad (7)$$

where $R = E/D$. Note that for purposes of comparing a simulated spectrum with no E/D distribution with one including the distribution (Eq. 7), ΔL in Gauss may be converted to its equivalent value in MHz using Eq. 4 as long as g' is specified (see Table II). Typically, the simulations reported here use ΔR values from 0.025 to 0.050 and the step size in R is 0.0025. (The range of $R_0 = E/D$ is 0–0.33). These large values of ΔR preclude using linewidth formulas based on first-order perturbation methods (25). Instead, an effective linewidth, ΔB_{eff}, due to distribution in E/D, for a particular molecular orientation may be calculated using Eq. 8.

$$\Delta B_{\text{eff}} = B_{(R_0-\Delta R)} - B_{(R_0+\Delta R)} \qquad (8)$$

Because ΔB_{eff} is strongly dependent on θ and ϕ as well as on ΔR, E/D-distribution can contribute unexpected features to a simulated lineshape. Fig. 2 illustrates this point. The effective linewidth, ΔB_{eff}, has been calculated as a function of the angle θ for $\phi = 0°$ (z-x plane) and $\phi = 90°$ (z-y plane). Clearly, when $\theta \simeq 40°$, the lineshape reverts to the residual linewidth, ΔL. The inset in Fig. 2 illustrates a case where changes in the residual linewidth have a marked effect on the lineshape and amplitude of the spectrum. Here, three different values of ΔL have been used in the simulation. The spectra in the inset have been scaled so that they represent equivalent numbers of molecules. The value of E/D for the calculations summarized in Fig. 2 is 0.20 and the middle doublet transition is shown. The effect of varying the residual linewidth on the calculated spectrum is less marked in some other cases. For instance, for the lowest doublet transition when E/D is near 1/3, changes in ΔL, with the other parameters of the E/D distribution held constant, result mainly in changes in the breadth of the tails of the lowest-field feature relative to the breadth at the maximum of this feature. These examples serve to illustrate that the residual linewidth is an important simulation variable even when distributions in E/D are used.

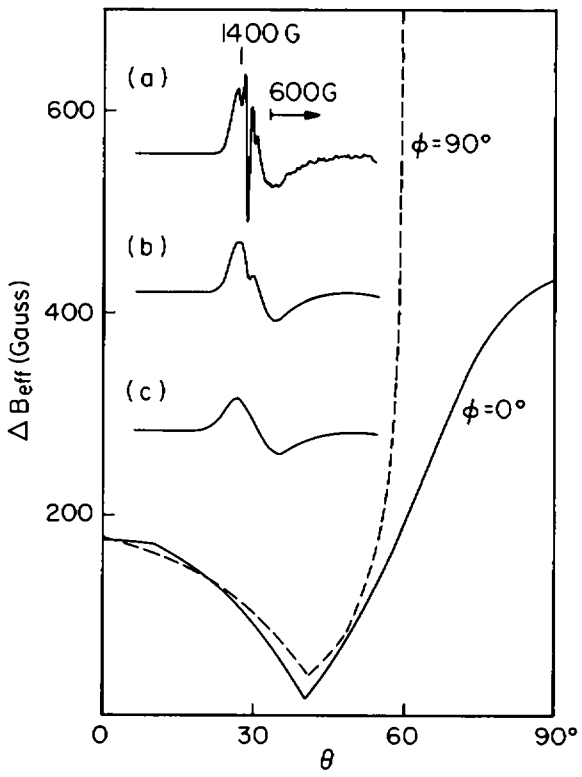

FIGURE 2 The effective linewidth, ΔB_{eff} resulting from E/D-distribution varies with molecular orientation. The variation at X-band of ΔB_{eff} with θ is shown here for values of ϕ of 0° and 90°. The calculation used an E/D-distribution (Eq. 7) with $R_0 = 0.20$, $\Delta R = 0.05$, and $D = 0.23$ cm^{-1}. The inset shows the effect of residual linewidth, ΔL, on a complete simulation using E/D-distribution. For the inset, ΔL was 43 G in *a*, 87 G in *b*, and 173 G in *c*. The amplitudes are adjusted to equivalent spin concentrations for each spectrum.

Experimental Samples

PAH was provided by L. M. Bloom and S. J. Benkovic (Pennsylvania State University) and was prepared from rat livers as described (1). The enzyme is in the ferric form after the preparation (1), and samples for EPR contained 5–25 mg/ml ($1–5 \times 10^{-4}$ M in iron) of enzyme in Tris-buffered saline (pH 7.25) with 50 μM EDTA. Paramagnetic resonance measurements on PAH at X-band were made as described (1) at temperatures near 4 K using a cryostat (model ESR-10, Oxford Instruments, Bedford, MA). Spectra at low frequencies (L-band, 1.153 GHz, and S-band, 3.429 GHz) were recorded on spectrometers at the National Biomedical ESR Center, Medical College of Wisconsin. As noted earlier (1), the specific activity of the enzyme in different preparations typically varies from 20 to 60% of the highest measured activity of 14.4 U/mg. More recently, this fractional activity has been shown not to be a function of the isolation procedure but is fixed at the earliest step in the preparation (2). EPR intensity at $g' = 4.3$ has been shown to correlate with fraction of inactive enzyme; that at $g' = 6.7$ is proportional to active enzyme (1). Samples that have been frozen for EPR and thawed lose no detectable activity and the error in activity measurements is usually

~10% (2). Glycerol cannot be used as a cryoprotectant for PAH because it is an inhibitor of the enzyme and alters the EPR spectrum drastically (1). 4-Fluorophenylalanine competes with the substrate in binding to PAH and reversibly changes the EPR spectrum in a manner similar to the change brought about by phenylalanine (1).

Human serum transferrin from Sigma Chemical Co. (St. Louis, MO) was dissolved at 2.5 mM in pH 7.0 bicarbonate (50 mM) containing 100 mM sodium perchlorate and mixed with two equivalents of iron from 0.1 M ferric nitrate in 0.1 M nitrilotriacetate (Aldrich Chemical Co., Milwaukee, WI). The solution was kept at 4°C for 1 d before dialysis into 50 mM Tris-50 mM bicarbonate, $pH^{20°}$ 7.0 or into 50 mM HEPES-50 mM bicarbonate, $pH^{20°}$ 8.0.

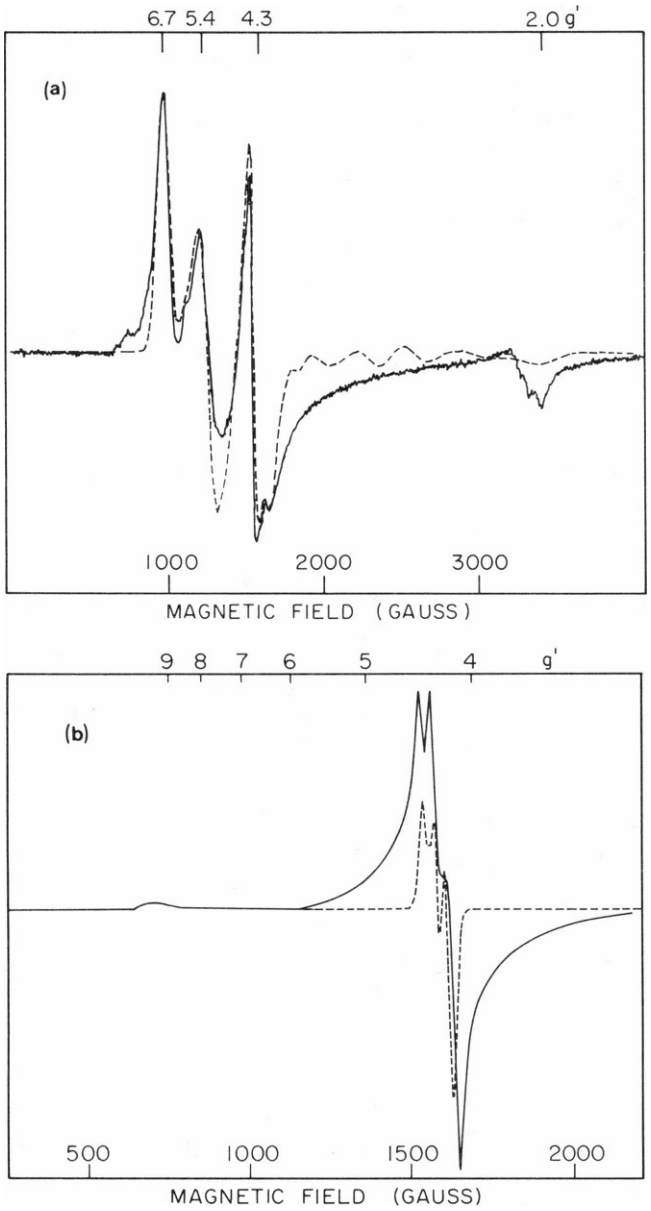

FIGURE 3 Simulations of spectra using ordinary lineshapes, a frequency-swept Gaussian (Eq. 6) for PAH and a field-swept Lorentzian for transferrin, are shown here in *a* for phenylalanine hydroxylase and in *b* for diferric, human transferrin. The parameters used in the simulations are given in Table I. The fit of experimental (*solid lines*) and simulated (*dashed lines*) spectra is not improved by using larger linewidths.

TABLE I
PARAMETERS FOR SIMULATIONS USING ORDINARY LINESHAPES

Sample	Transition‡	E/D	D	$\Delta\nu$*	ΔB	g'
			cm^{-1}	*MHz*	*Gauss*	
Phenylalanine hydroxylase						
Component I	Lowest (83%)	0.032	1.0	447	48	(6.7)
Component II	Middle (14%)	0.300	0.28	306	51	(4.3)
Component III	Middle (3%)	0.333	0.37	188	31	(4.3)
Diferric transferrin						
	Middle	0.326	0.25	84	14	(4.3)

*The lineshape was a Gaussian, frequency-swept one for the PAH simulation and a Lorentzian field-swept one for transferrin. The relation between $\Delta\nu$ and ΔB is given in Eq. 4.
‡Transitions between levels in the lowest Kramers doublet are designated by lowest; those in the middle doublet by middle. Percents refer to relative spin concentrations.

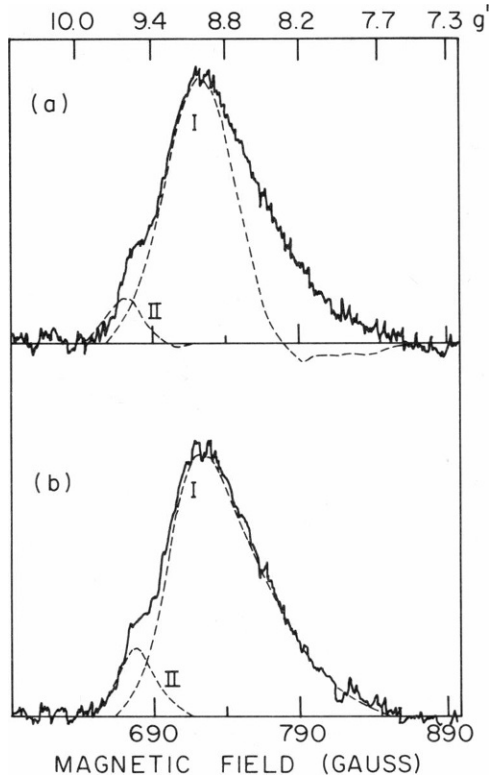

FIGURE 4 Two lineshapes are used to simulate the low-field features from the EPR of the lowest Kramers doublet transition of transferrin. In *a*, Gaussian, frequency-swept lineshapes of widths, $\Delta\nu$, 377 and 194 MHz for sites I and II were used. E/D-values were 0.18 and 0.29 for the two sites. The calculation includes summation over θ and ϕ. In *b*, an E/D-distribution (Eq. 7) was used. For site I, $R_0 = 0.190$ and $\Delta R = 0.039$; for site II, $R_0 = 0.325$ and $\Delta R = 0.050$. The residual linewidth, δL, was 5.2 Gauss. The simulation was for $\theta = \phi = 90°$ (i.e., B_0 is aligned with the y-principal axis of the g'-tensor). The experimental sample contained 1.6 mM transferrin in 0.05 M HEPES, 0.05 M bicarbonate, and 0.5 M sodium chloride, pH 8.0. The experimental spectrum was recorded at 130 K.

RESULTS

For X-band EPR spectra with $S = 5/2$, the positions of maxima are a strong function of the ratio E/D but depend on D only when the magnitude of this parameter is on the order of the X-band quantum or smaller. In the other case, when D is much larger than $h\nu_0$, excited state admixture with the ground states leads to the "other terms" in Eq. 1 and to shifts in maxima. The general effects of E/D and small D on X-band spectra of pure $S = 5/2$ are shown in the Appendix. The magnitude of D used in the final simulations of transferrin spectra is 0.23 cm^{-1}, which is similar to most reported values for the component of the sample giving the sharp signal (28, 29). The D-value for the sharp components of the PAH spectrum is ~1 cm^{-1} based on comparison of X- and Q-band EPR and on temperature dependence of signal intensity at $g' = 6.7$ and 5.3 (Mavrophilipos, D. V., unpublished observations). In the absence of experimental information on the D-values of the broad components of the signals from either protein, it seems reasonable to estimate that D is similar for the broad and sharp components. With these values of D, the positions of the major maxima and minima in the experimental spectra of PAH and transferrin are readily simulated using the first three terms of Eq. 1. This point is illustrated in Fig. 3 *a* for PAH and 3 *b* for transferrin, but deficiencies in the simulation are also apparent. The broad tails of the features in the $g' = 4.3$ region represent a large fraction of

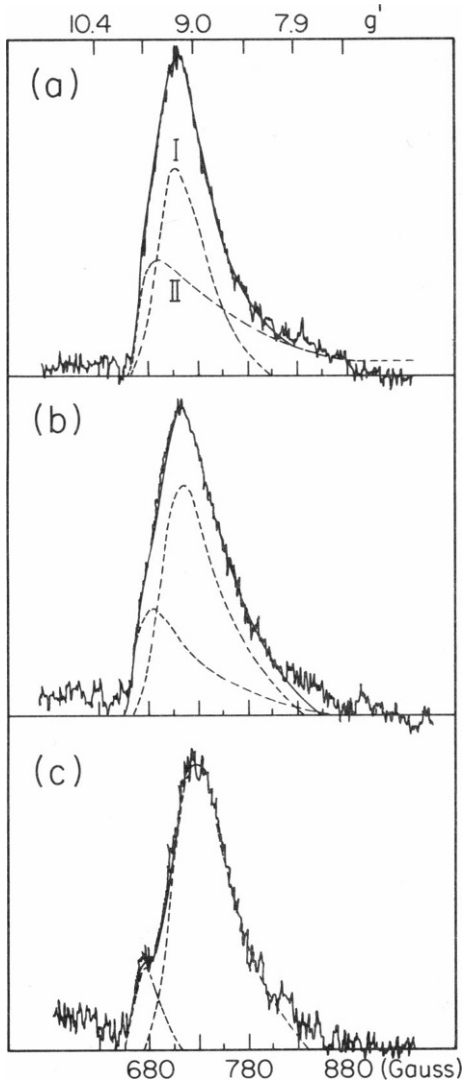

FIGURE 5 The low-field region of experimental and simulated spectra of diferric transferrin at three salt concentrations is shown for (*a*) no salt, (*b*) 0.19 M sodium chloride, and (*c*) 0.5 M sodium chloride. The samples contained 2.5, 2.3, and 2.1 mM transferrin, respectively, 50 mM Tris and 50 mM sodium bicarbonate at pH 7.0. The dashed lines show the two components of a simulation using the E/D-distribution model; the solid line that is superimposed on the experimental spectrum is the sum of the two simulations. Values of R_0 (ΔR) for the calculations were (*a*) site I, 0.220 (0.040); site II, 0.325 (0.120); (*b*) site I, 0.205 (0.045); site II, 0.325 (0.100); and (*c*) site I, 0.185 (0.036); site II, 0.325 (0.050). The residual linewidth, ΔL, was 5.2 Gauss. The simulation is a partial one with $\theta = \phi = 90°$.

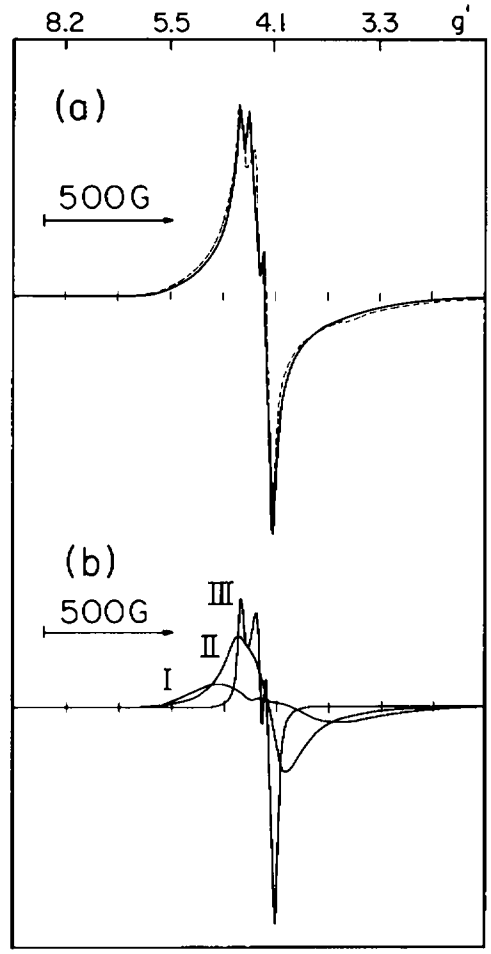

FIGURE 6 A portion of the experimental spectrum of diferric transferrin is compared in *a* with a simulation of the middle Kramers doublet transition (*dashed line*) using the E/D-distribution model for the lineshape. The simulation in *a* is the sum of the three calculations shown in *b*. Conditions for the experimental spectrum are given in Fig. 5 *a*. Table II gives the simulation parameters.

TABLE II
PARAMETERS FOR SIMULATIONS USING E/D DISTRIBUTION

	Transition‡	E/D	R_0	ΔR	D	$\Delta\nu$	ΔB	ΔL
					cm^{-1}	*MHz*	*Gauss*	*Gauss g'*
Transferrin (Fig. 6)								
Component I*	Middle (46%)	—	0.22	0.04	0.23	524	—	87 (4.3)
Component II*	Middle (48%)	—	0.325	0.12	0.23	313	—	52 (4.3)
Component III§	Middle (6%)	0.325	—	—	0.23	84	14	— (4.3)
PAH (Fig. 7)								
Component I*	Middle (57%)	—	0.333	0.08	0.6	524	—	87 (4.3)
Component II*	Middle (38%)	—	0.11	0.05	0.6	524	—	87 (4.3)
Component III§	Middle (3%)	0.333	—	—	0.37	104	17	— (4.3)
Component IV§	Middle (2%)	0.333	—	—	0.27	157	26	— (4.3)
PAH (Fig. 8)								
Component I*	Middle (51%)	—	0.20	0.05	0.6	524	—	87 (4.3)
Component II‖	Lowest (41%)	0.032	—	—	0.6	447	48	— (6.7)
Component III§	Middle (3%)	0.333	—	—	0.37	208	35	— (4.3)
Component IV§	Middle (5%)	0.30	—	—	0.28	313	52	— (4.3)

*R_0 and R are defined in Eq. 8. The relation between $\Delta\nu$ and ΔB is given in Eq. 4.
‡Transitions between levels in the lowest Kramers doublet are designated by lowest; those in the middle doublet by middle. Percents refer to relative spin concentrations.
§A Lorentzian, field-swept line was used.
‖A Gaussian frequency-swept line was used.

the intensity of the spectra, but simulations using the ordinary lineshapes (Eqs. 5 and 6) give little intensity in these regions. The aim of this report is to account for the full intensity of the regions of the EPR of PAH and transferrin shown in Fig. 3. Using linewidths greater than those used in the simulations represented in this figure is not sufficient. Distribution in parameters in the Hamiltonian Eq. 1 is suggested by the marked asymmetry of the experimental lines in the $g' = 4.3$ region of the spectra in Fig. 3.

Transferrin serves as an excellent model for testing methods of accounting for the broad features around $g' = 4.3$ in EPR spectra because the low-field ($\sim g' = 9$) extremum from the lowest Kramers doublet transition is well separated from the $g' = 4.3$ absorption resulting from the middle doublet transition. Any line-shape model that fits the $g' \simeq 9$ extremum for the lowest doublet transition should also provide an adequate fit to the signal for the middle doublet transition. Inspection of the low field extremum of the transferrin spectrum reveals that there are at least two components contributing to it, as has been noted by other authors (4, 30–32). Fig. 4 gives two simulations of the low field extremum for transferrin; each simulation invokes two components but the lineshapes used differ. Fig. 4 *a* results from summation of spectra over θ and ϕ and use of ordinary, frequency-swept Gaussian lineshapes. The linewidths, in frequency units, of the two components differ by about a factor of two. The relative number of molecules contributing to the species labeled components I and II are calculated by weighting by the appropriate transition probability. For Fig. 4 *a*, 25 and 75% ($\sim \pm 5\%$) of the spins contribute to sites II and I, respectively. In contrast, an E/D-distribution simulation of the transferrin low-field feature is shown in Fig. 4*b*. The populations of sites II and I in this simulation are 30 and 70%. The values of E/D and the linewidths used in the calculations are given in the legend to Fig. 4. The simulations in Fig. 4 *b* are partial simulations at $\theta = \phi = 90°$ (along the y-principal axis of the g-tensor). Summation over θ and ϕ has very little effect on the shape of this region of the spectrum if a distribution in E/D is used in the simulation.

The EPR lineshape of transferrin is salt- and pH-dependent. This dependence provides an opportunity for further evaluation of the efficacy of E/D-distribution analysis. The approach gives good fits to features of the lowest doublet transition in experimental spectra at three salt concentrations. Fig. 5 shows the simulation for the low-field region of this transition. The ratios of the occupancy of site I to site II, based on the simulation, are 1.0, 1.2, and 2.3 at 0, 0.19 M, and 0.5 M salt, respectively. It is also known that iron is lost from transferrin at low pH (32), with one site giving up the metal more readily than the other. Spectra of transferrin samples prepared by adjusting pH and with no added salt have also been recorded (spectra not shown). The spectra can be simulated using a ratio of spins in sites I and II of 0.94, 0.26, and 0.24 for samples at pH values of 7.0, 5.0, and 3.0, respectively. Because the E/D-distribution parameters, R_0 and ΔR, vary only slightly for samples at different pH values, the pH-dependent spectra provide confirmation of the choice of parameters for simulating sites I and II in Fig. 5 *a*.

Each set of parameters used for the partial simulation shown in Fig. 5 also was used, with the exception of

linewidth, in a simulation of the EPR from the middle Kramers doublet transition for the same sample. The result of the calculation for the no-salt sample is shown in Fig. 6. Good fits were also obtained using parameters given in the legend to Fig. 5 to simulate the middle doublet transitions of samples with salt. (The simple Gaussian lineshape model gave a very poor fit to the transferrin features in the $g' = 4.3$ region [spectrum not shown].) Note that in Fig. 6, a third, sharp component has been added to account for prominent features near $g' = 4.3$. This component, although making a strong contribution to the appearance of the spectrum near $g' = 4.3$, represents only an estimated 6% of the molecules present (see Table II). This component makes no significant contribution to the low-field peak of the lowest Kramers doublet transition. The combined simulations in Figs. 5 *a* and 6 also give relative intensity of the partial spectrum from the lowest doublet transition at $g' = 9.0$ to intensity of the portion of the middle doublet spectrum at $g' = 4.3$ identical to the experimental ratio. To achieve good fits, it was necessary to use a linewidth at $g' = 4.3$ of 524 MHz for simulation of the middle Kramers doublet transition (Fig. 6), while a width of 65 MHz was best for simulating the lowest doublet transition (Fig. 5).

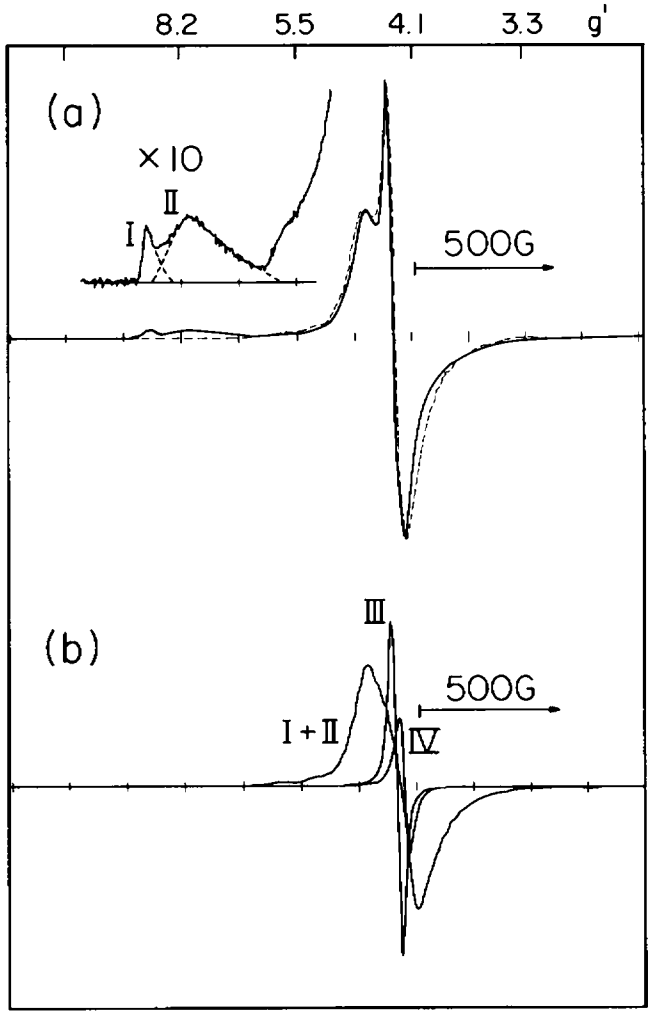

FIGURE 7 Simulation (*dashed line*) of the EPR spectrum of PAH in the presence of inhibitor (4-fluorophenylalanine) is compared with experiment (*solid line*). The inset in *a* shows a 10-fold amplification of the low-field region of the spectrum. This region was used to determine the relative amounts of the two major ferric species in this protein using the *E/D*-distribution (Eq. 8) lineshape. The same proportions of major components were then used to simulate the absorption around $g' = 4.3$ for the middle doublet as shown in *a*. Small amounts of two sharp components were also added to the simulation. The individual components which were summed to give *a* are shown in *b*. The experimental spectrum was recorded at ~6 K. Simulation parameters are given in Table II.

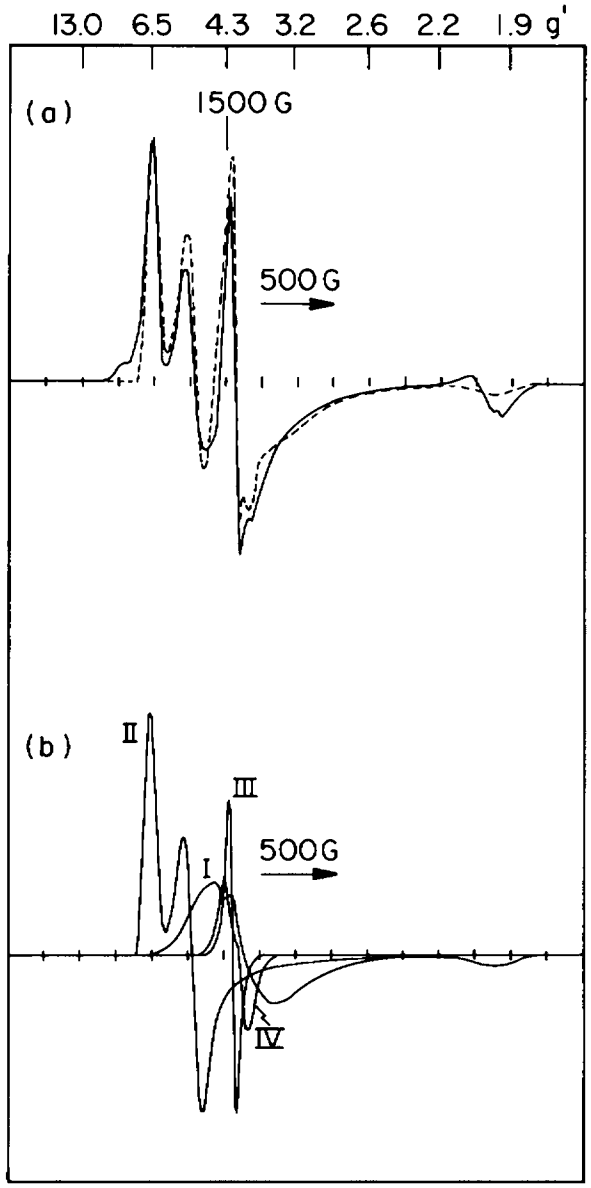

FIGURE 8 Experimental and simulated EPR spectra of PAH in the resting state are shown. The experimental spectrum (*solid line*) was redrawn from Wallick et al. (1). The simulated spectrum (*dashed line*) had nearly the same proportion of components I and II as that in Fig. 7. The individual calculated spectra are shown in *b*. The experimental spectrum was recorded at ~6 K. Simulation parameters are given in Table II.

As a test of the accuracy of using an E/D-distribution simulation to account quantitatively for the spin concentration in each part of a two component spectrum, simulations of spectra from the lowest doublet transition of transferrin samples in the presence or absence of salt were compared. Spectra of 1.6 mM transferrin in 50 mM HEPES buffer, 50 mM bicarbonate, pH 8.0, were measured. The sample was then brought to 1.33 mM in protein and 0.5 M sodium chloride by addition of 3.0 M salt and a second set of spectra were obtained. As noted above, the parameters for the simulation and the occupancy of sites I and II change with additions of salt. However, when the spin concentration is determined for the sum of contributions from sites I and II for the two samples, with appropriate adjustment for dilution, the computation gives a ratio of total spins in the high salt sample to those in low salt of 0.97 ± 0.05. That no iron was lost from the protein on addition of salt was demonstrated by dialysis of the high-salt sample into no-salt buffer and comparison of the EPR signals before the salt addition and after dialysis. The lineshapes were the same and the spectral intensities, normalized by protein determination, were identical within the limits of reproducibility of signal intensity when a sample is positioned in the cavity several times (~±5%).

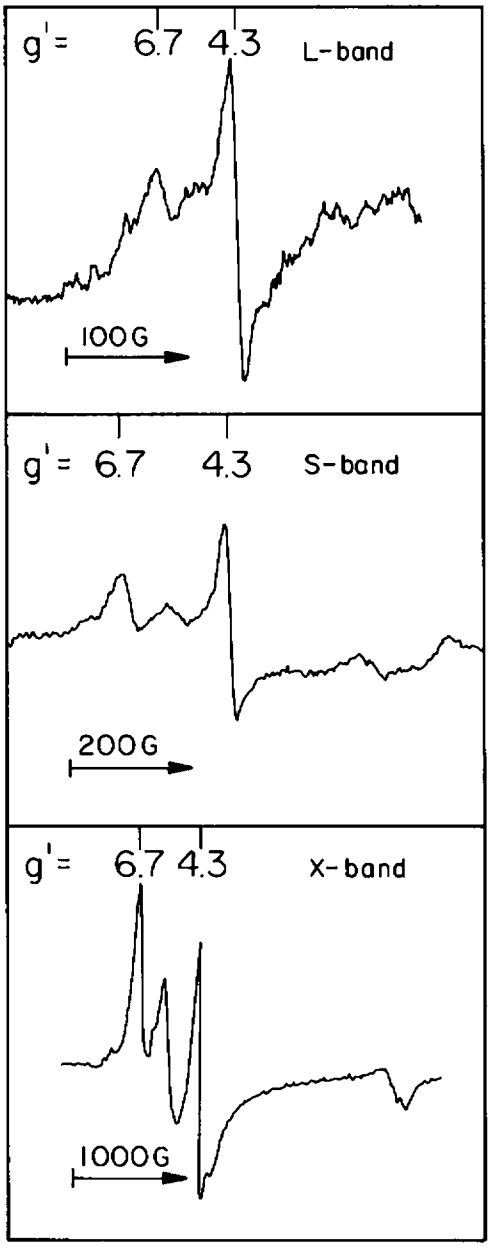

FIGURE 9 The EPR spectra of PAH were recorded at three frequencies: L-band (1.161 GHz), S-band (3.276 GHz), and X-band (9.234 GHz). The instrument settings for the spectra shown were for L-band: power, 25 dB; gain, 4×10^3; modulation amplitude, 10 Gauss; time constant and scan time, 1 s and 16 min; S-band: 20 dB; 4×10^3; 12.5 Gauss; 3 s and 30 min, respectively; X-band: 37 dB; 8×10^3; 20 Gauss; 0.128 s and 16 min, respectively. The L- and S-band samples were at 5.6 K and the X-band one at 5 K. A loop-gap resonator was used at L- and S-bands (33). The protein concentration was 9 mg/ml for L- and S-band samples and was 20 mg/ml for X-band. Note the different scan widths indicated on each spectrum. The X-band spectrum is taken from reference 1.

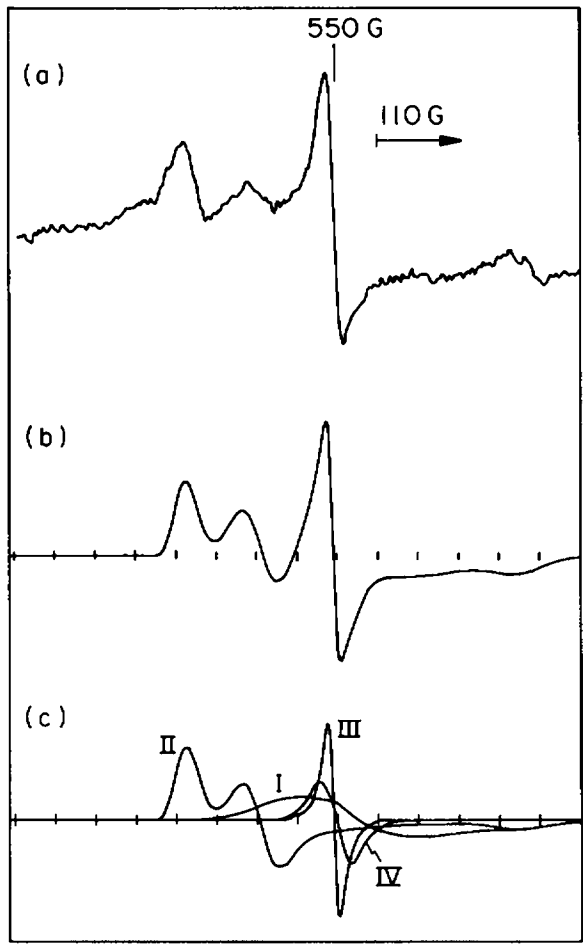

FIGURE 10 A simulation of the S-band EPR spectrum of PAH in the resting state is shown. The simulation parameters were the same as those used for the spectra shown in Fig. 8 except that here, the microwave frequency is 3.27 GHz and all the linewidths are reduced from those for the X-band calculation by a factor of three. The simulation in *b* is composed of components I-IV (see Fig. 8 and Table II). The simulations in *c* are the individual calculated spectra. The relative ratios for component I, II, III, and IV are 49, 40, 5, and 6%, respectively.

Simulation of spectra for PAH in the resting state is more complicated than is simulation of transferrin spectra because, for PAH, the low-field features of the component with $E/D \sim 1/3$ are overwhelmed by the more prominent features of the component with $E/D = 0.032$, making it difficult to fit both the lowest and middle doublet transitions independently. However, when the inhibitor, 4-fluorophenylalanine, is added to PAH, the $E/D = 0.032$ component is abolished and only $E/D \sim 1/3$ components remain. It is therefore possible to use the same approach to simulation of the EPR of the PAH-inhibitor complex as was used above for transferrin. The inset in Fig. 7 shows that the low-field region of the spectrum for this form of PAH can be simulated using the sum of two components and the E/D-distribution lineshape (Eq. 7) for both sites. Based on the simulation, the relative amounts of the two species of iron are 60% in site I and 40% in site II. To account for the details of the middle doublet transition shown in Fig. 7, small amounts of sharp features at $g' = 4.3$ have to be added and this brings the occupancy of sites I and II to 57 and 38%, respectively. Finally, the spectrum of resting PAH was simulated using almost the same relative proportions of major components that were used for the enzyme–inhibitor complex spectrum of Fig. 7. The result is shown in Fig. 8 (parameters given in Table II).

The mechanism of the inhomogeneous line broadening that contributes to the spectrum of PAH can be examined further in experiments performed at several microwave frequencies. Experimental spectra of native PAH have been obtained at three frequencies (X-, S-, and L-bands) and these are compared in Fig. 9. For the $g' = 6.7$ feature (part of component II, Fig. 8 *b*), extrapolation of the low-field half-width at half-height to zero frequency gives $\Delta\nu = 66$ MHz (equivalent to 7.0 Gauss at $g' = 6.7$) as the frequency-independent component. The frequency-dependence of the linewidth of this PAH component and simulations using Eq. 6 are consistent with a broadening mechanism similar to those discussed in terms of g'-strain (26, 27) and a frequency-independent residual linewidth. By comparison, component I, which made an obvious contribution to the X-band spectra (Fig. 8), cannot immediately be discerned in the S- and L-band spectra of Fig. 9. A simulation of the S-band spectrum shown in Fig. 9 also has been done by including components I–IV of Fig. 8 *b* and by using parameters in Table II and $\nu_0 = 3.276$ GHz. The linewidths for the S-band simulation were taken as decreasing linearly with frequency. The simulation (Fig. 10) shows that the minor, sharp components (III and IV) dominate the PAH spectrum in the $g' = 4.3$ region at lower frequencies and the broad feature (component I) is virtually lost in the baseline when it is simulated using a distribution in E/D. The relative intensities of the prominent features of the S-band spectra are approximated well by the simulation, which lends support to the choice of E/D distribution as a lineshape contribution.

CONCLUSION

The aim of this calculation has been to estimate the proportions of molecules in the two iron environments in PAH. The fractional specific activity of the PAH sample used for Figs. 7 and 8 was 36% ± 4% and, as reported elsewhere (2), the simulations suggest that 41% ± 5% of the iron is in the site designated II (Table II), supporting the assignment of this site to active enzyme. Other simulations using parameters that vary slightly from those given in Table II give a range of spin concentrations in site II ranging from 37 to 41% of the total. The accuracy of the analysis of the distribution of iron between two sites depends on the extent to which quantitation is independent of the lineshape model. Using the E/D-distribution model, the quantitation method has been tested by comparing the spin concentration derived from simulations of transferrin at several salt concentrations. The calculated spin concentration was constant, although specific parameters in the simulation varied. In the case of PAH, approximately the same relative occupancy of two major sites was obtained for samples with very different lineshapes: the resting enzyme and the inhibitor-saturated protein. Nevertheless, it remains possible that another lineshape model could lead

TABLE III
SECULAR DETERMINANT ASSOCIATED WITH THE SPIN HAMILTONIAN EQ. 1

	$\lvert 5/2\rangle$	$\lvert -3/2\rangle$	$\lvert 1/2\rangle$	$\lvert -5/2\rangle$	$\lvert 3/2\rangle$	$\lvert -1/2\rangle$
$\langle 5/2\rvert$	$3.33D + \frac{5}{2} g\mu_B B_0 \cos\theta$	0	$3.16\lambda D$	0	$g\mu_B B_0 \sin\theta \sqrt{5/2}$ $(\cos\phi - i\sin\phi)$	0
$\langle -3/2\rvert$	0	$-0.67D - \frac{3}{2} g\mu_B B_0 \cos\theta$	$4.24\lambda D$	$g\mu_B B_0 \sin\theta \sqrt{5/2}$ $(\cos\phi - i\sin\phi)$	0	$g\mu_B B_0 \sin\theta \sqrt{2}$ $(\cos\phi + i\sin\phi)$
$\langle 1/2\rvert$	$3.16\lambda D$	$4.24\lambda D$	$-2.67D + \frac{1}{2} g\mu_B B_0 \cos\theta$	0	$g\mu_B B_0 \sin\theta \sqrt{2}$ $(\cos\phi + i\sin\phi)$	$g\mu_B B_0 \sin\theta \frac{3}{2}$ $(\cos\phi - i\sin\phi)$
$\langle -5/2\rvert$	0	$g\mu_B B_0 \sin\theta \sqrt{5/2}$ $(\cos\phi + i\sin\phi)$	0	$3.33D - \frac{5}{2} g\mu_B B_0 \cos\theta$	0	$3.16\lambda D$
$\langle 3/2\rvert$	$g\mu_B B_0 \sin\theta \sqrt{5/2}$ $(\cos\phi + i\sin\phi)$	0	$g\mu_B B_0 \sin\theta \sqrt{2}$ $(\cos\phi - i\sin\phi)$	0	$-0.67D + \frac{3}{2} g\mu_B B_0 \cos\theta$	$4.24\lambda D$
$\langle -1/2\rvert$	0	$g\mu_B B_0 \sin\theta \sqrt{2}$ $(\cos\phi - i\sin\phi)$	$g\mu_B B_0 \sin\theta \frac{3}{2}$ $(\cos\phi + i\sin\phi)$	$3.16\lambda D$	$4.24\lambda D$	$-2.67D - \frac{1}{2} g\mu_B B_0 \cos\theta$

to significantly different conclusions about the spin concentration in multicomponent samples. Spectral distortions resulting from effectively anisotropic linewidth terms, exemplified in Fig. 2, are a particular concern in simulations of cases where several spectra overlap.

The calculations shown in Figs. 11 and 12 (Appendix) illustrate that distribution in D might also be considered as a source of broad and asymmetric lineshapes, although the line-broadening effects of D-distribution would be smaller than those of E/D-distribution. In fact, in spectra where features from both the lowest and the middle Kramers doublets are apparent, best fits are obtained when the residual linewidth, ΔL, for simulation of the lowest doublet transition is about ten times smaller than the residual linewidth used for simulation of the middle doublet transition. Comparison of parameters for Fig. 5 with those of Fig. 6 or of those for Fig. 7 with ones of the inset of the same figure illustrates this point. These cases clearly indicate that some line-broadening mechanism in addition to E/D-distribution exists. Simulations using D-distribution indeed show that the low-field feature from the lowest doublet transition is virtually unaffected by a distribution in D, while the feature at $g' = 4.3$ from the middle doublet transition is broadened considerably if a distribution around $D \leq 0.3$ cm^{-1} is used in an X-band simulation. Thus, while E/D-distribution provides the only good fit for the features around $g' = 9.0$, several lineshape approaches, including D-distribution, could be used in simulating $g' = 4.3$ features. A detailed calculation involving both D- and E/D-distributions has not been made because of prohibitive length of the computation. Line broadening by D-distribution should decrease considerably at lower fields.

Other authors have considered problems similar to the ones discussed here in simulating broad, asymmetric lineshapes. The transformation from frequency-swept to field-swept spectra (20, 21) does not account for the marked asymmetry in the $g' = 4.3$ region of the spectra of PAH or transferrin. What evidence there is at present for the magnitude of D for these proteins indicates that the EPR spectra represent pure high-spin states, so that a distribution of excited state admixture with the ground, $^6A_1$ state (5–7) also seems an unlikely explanation for asymmetry and breadth of the lineshapes.

APPENDIX

Because most previous simulations of high-spin iron spectra are limited to plots of g'-values vs. various simulation variables, the results of some spectral simulations for the low-field region of cases that use the spin

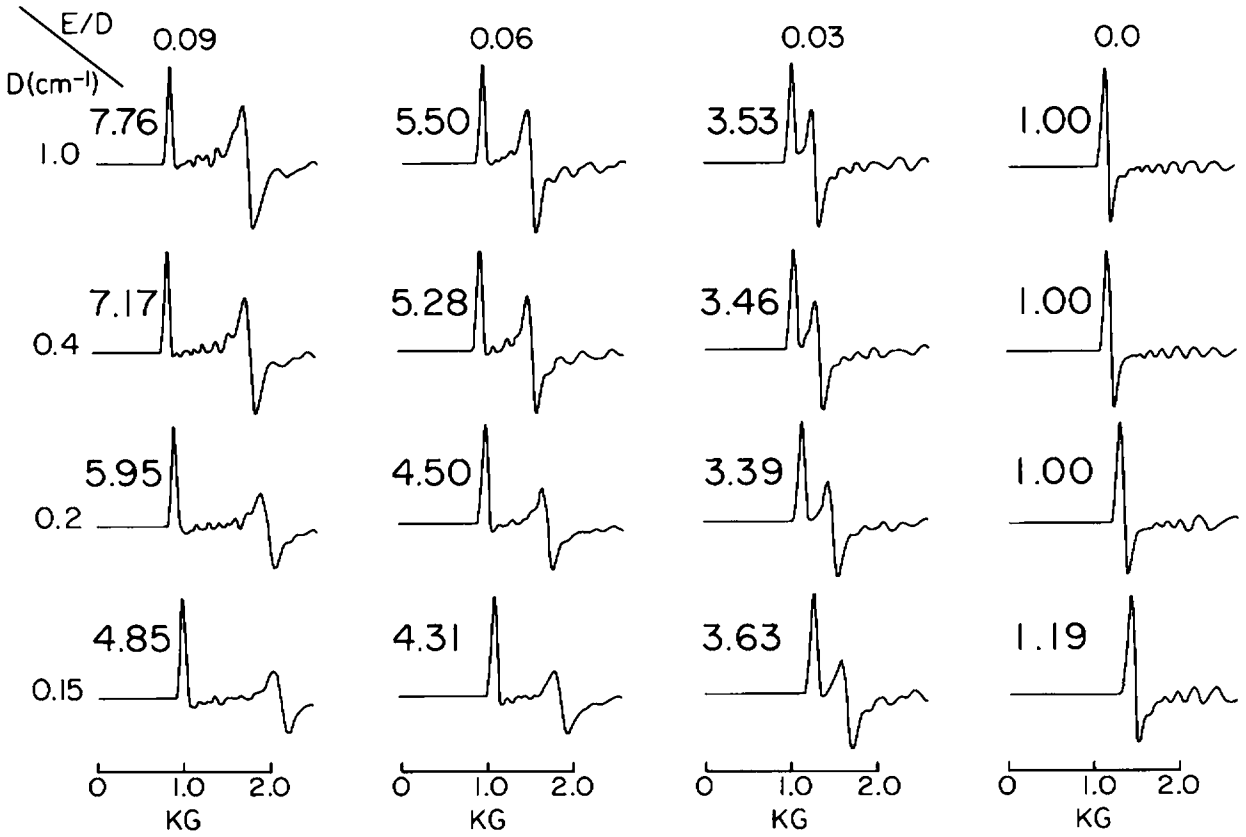

FIGURE 11 Simulated X-band EPR spectra are shown for transitions within the lowest Kramers doublet for values of the spin Hamiltonian parameters D and E/D. The microwave frequency was 9.3 GHz. Computations were performed over intervals of 5° in θ and ϕ. The mosaic ripple in the spectra can be eliminated by decreasing the angular steps to 2°. The lineshape is frequency-swept Gaussian with half-width at half-height of 353 MHz. The amplitudes of the spectra are normalized to the same magnitude for the low-field maximum. The relative number of molecules required to give the intensity shown is indicated by the number on the left side of the individual spectra.

Hamiltonian Eq. 1 are given here. Table III gives the secular determinant associated with Eq. 1 when "other terms" are negligible.

Fig. 11 shows a series of simulated, partial X-band EPR spectra for the lowest Kramers doublet of a spin 5/2 system. Only the regions giving features as the y- and x-principal values of the g'-tensor are shown. In looking down each row in the figure, it is seen that the maxima in the spectra begin to shift for D-values < 0.6 cm^{-1}. The appearance of the lineshape for different values of E/D is seen by viewing the figures from left to right along a row. The "ripples" in Fig. 11 are computational as noted earlier. Fig. 12 shows a display for the resonance from the middle Kramers doublet. In this case, E/D is only varied by a small amount (0.3–0.333) and, for D values less than 0.4 cm^{-1}, the spectra vary strongly with D.

Fig. 13 illustrates the effect of anisotropic transition probability and g-values on the intensity of the low-field feature for the lowest Kramers doublet transition for spin 5/2 spectra with E/D varying from 0 to $\frac{1}{3}$. This figure serves as a rough guide to estimating the fraction of components with different E/D-values, assuming that linewidths are constant. The figure also makes clear why it is necessary to use all possible means of enhancing signal intensity (concentrated samples, low temperature, optimum microwave frequency, etc.) when examining $S = 5/2$ samples with E/D-values near 1/3.

We are grateful to Avram Edidin for initial simulations of the PAH spectrum shown in Fig. 3 *a*.

This project was supported by BRSG grant S07-RR07041 awarded by the Biomedical Research Support Grant Program, Division of Research Resources, National Institutes of Health (NIH) and by NIH grant R01-GM36232. The spectra at L- and S-bands (Fig. 9) were recorded at the National Biomedical ESR Center, Medical College of Wisconsin, Milwaukee with support provided by grant RR-01008.

Received for publication 24 February 1986 and in final form 26 August 1986.

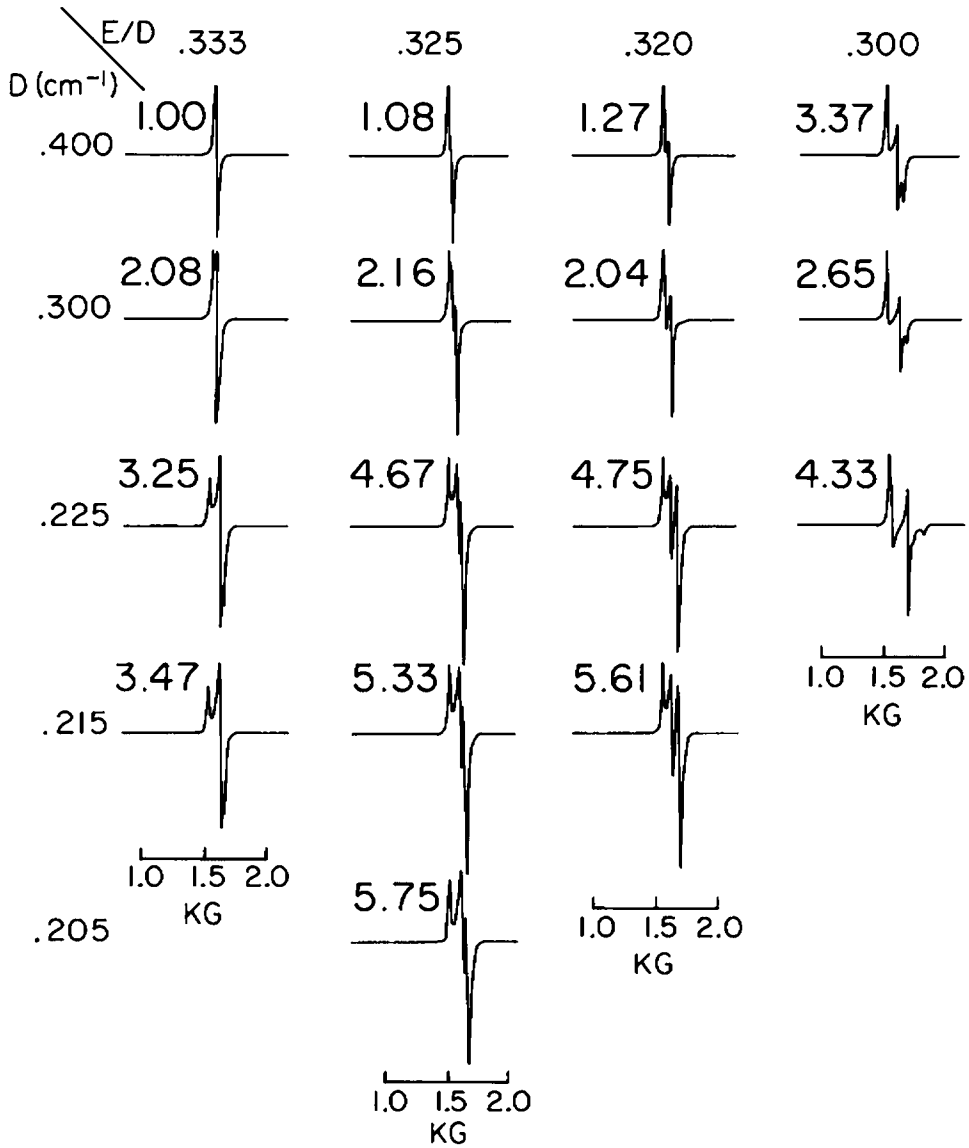

FIGURE 12 X-Band EPR spectra from the middle Kramers doublet transition are simulated for $\lambda \ll 1/3$ and for different D and E/D-values. The microwave frequency is 9.3 GHz. The absorption line shape is a Lorentzian field-swept shape with $\Delta B = 10.4$ Gauss. Spectra are normalized to equal amplitudes of the largest maximum above the baseline. Proportions of molecules are indicated as they were for Fig. 11.

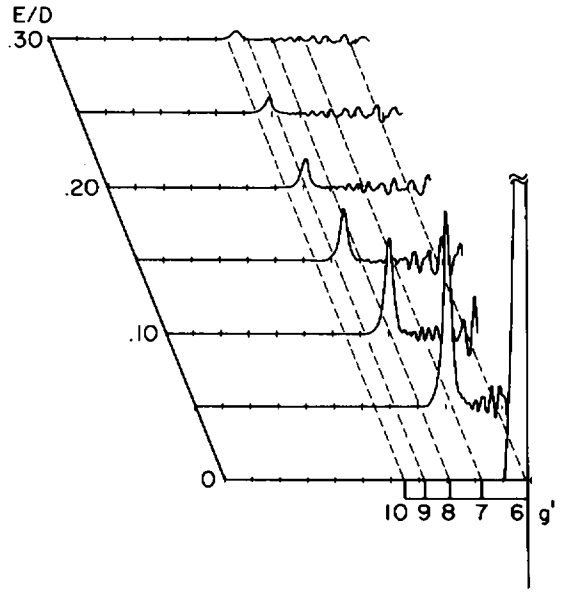

FIGURE 13 The effect of anisotropic transition probabilities on low-field features of $S = 5/2$ EPR spectra is illustrated. Only the low-field feature from the lowest Kramers doublet transition is shown and each spectrum is normalized to the same spin concentration. For the simulation, $D = 2.0\ cm^{-1}$, $\nu_0 = 9.07$ GHz, field-swept Lorentzian lineshape with half-width at half-height = 14 G and the mesh of θ and $\phi = 3°$. The peak at $g' = 6.0$ reaches a maximum at a point three times higher than the height at which it is truncated in the figure.

REFERENCES

1. Wallick, D. E., L. M. Bloom, B. J. Gaffney, and S. J. Benkovic. 1984. Reductive activation of phenylanaline hydroxylase and its effect on the redox state of the non-heme iron. *Biochemistry.* 23:1295–1302.
2. Bloom, L. M., S. J. Benkovic, and B. J. Gaffney. 1986. Characterization of phenylalaning hydroxylase. *Biochemistry.* 25:4204–4210.
3. Price, E. M., and J. F. Gibson. 1972. Electron paramagnetic resonance evidence for a distinction between the two iron-binding sites in transferrin and in conalbumin. *J. Biol. Chem.* 247:8031–8035.
4. Folajtar, D. A., and N. D. Chasteen. 1982. Measurement of non-synergistic anion binding to transferrin by EPR difference spectroscopy. *J. Am. Chem. Soc.* 104:5775–5780.
5. Brill, A. S., F. G. Fiamingo, and D. A. Hampton. 1978. Characterization of high-spin ferric states in heme proteins. *In* Frontiers in Biological Energetics. Vol. 2. P. L. Dutton, editor. Academic Press, Inc., New York. 1025–1033.
6. Maltempo, M. M. 1976. The spin 3/2 state and quantum spin mixtures in haem proteins. *Quart. Rev. Biophys.* 9:181–215.
7. Ristau, O. 1981. Analysis of magnetic properties of ferric hemoproteins: high spin-low spin equilibrium in cytochrome P-450. *Period. Biol.* 83:39–49.
8. Wickman, H. H., M. P. Klein, and D. A. Shirley. 1965. Paramagnetic resonance of Fe^{3+} in polycrystalline ferrichrome A. *J. Chem. Phys.* 42:2113–2117.
9. Swalen, J. D., and H. M. Gladney. 1964. Computer analysis of electron paramagnetic resonance spectra. *IBM J.* November (1964):515–516.
10. Brumby, S. 1983. Computer simulation of magnetic resonance spectra. *Mag. Reson. Rev.* 8:1–32.
11. Dowsing, R. D., and J. F, Gibson. 1969. Electron spin resonance of high-spin d^5 system. *J. Chem. Phys.* 50:294–303.
12. Aasa, R. 1970. Powder lineshapes in the electron paramagnetic resonance spectra of high-spin ferric complexes. *J. Chem. Phys.* 52:3919–3930.
13. Sweeney, W. V., D. Coucouvanis, and R. E. Coffman. 1973. ESR of spin 5/2 systems with axial symmetry and moderately large zero-field splittings. Application of line-shape calculations to the interpretation of random oriented microcrystallite spectra. *J. Chem. Phys.* 59:369–379.
14. Dowsing, R. D., and D. J. E. Ingram. 1969. Simulation of the electron spin resonance spectra of polycrystalline samples. *J. Magn. Res.* 1:517–323.
15. Scullane, M. I., L. K. White, and N. D. Chasteen. 1982. An efficient approach to computer simulation of EPR spectra of high-spin Fe(III) in rhombic ligand fields. *J. Magn. Res.* 47:383–397.
16. Nettar, D., and J. J. Villafranca. 1985. A program for EPR powder spectrum simulation. *J. Magn. Res.* 64:61–65.
17. McGavin, D. G., and W. C. Tennant. 1985. Analysis and computer simulation of high-spin Fe^{3+} powder EPR spectra with g_{iso} approximately 30/7. *J. Magn. Res.* 62:357–369.
18. Aasa, R., and T. Vänngard. 1975. EPR signal intensity and powder shapes: a reexamination. *J. Magn. Res.* 19:308–315.
19. Van Veen, G. 1978. Simulation and analysis of EPR spectra of paramagnetic iron in powders. *J. Magn. Res.* 30:91–109.
20. Pilbrow, J. R., G. R. Sinclair, D. R. Hutton, and G. J. Troup. 1983. Asymmetric lines in field-swept EPR: Cr^{3+} looping transitions in ruby. *J. Magn. Res.* 52:386–399.
21. Pilbrow, J. R. 1984. Lineshapes in frequency-swept and field-swept EPR for spin 1/2. *J. Magn. Res.* 58:186–203.
22. Brill, A. S., Fiamingo, F. G., Hampton, D. A., Levin, P. D., and R. Thorkildsen. 1985. Density of low-energy vibrational states in a protein solution. *Phys. Rev. Lett.* 54:1864–1867.
23. Coffman, R. E. 1975. Inhomogenous broadened lineshapes and information content of calculated paramagnetic resonance spectra of biological molecules containing high-spin iron (III). *J. Phys. Chem.* 79:1129–1136.
24. Calvo, R., and G. Bemski. 1976. On the electron spin resonance linewidths of metmyoglobin. *J. Chem. Phys.* 64:2264–2265.
25. Ja, Y. H. 1970. Anisotropic broadening of the linewidth of the electron paramagnetic resonance spectrum of Fe^{3+} in petalite, $LiAlSi_4O_{10}$. *Aust. J. Phys.* 23:445–448.
26. Hagen, W. R. 1981. Dislocation strain broadening as a source of anisotropic linewidth and asymmetrical lineshape in the electron paramagnetic resonance spectrum of metalloproteins and related systems. *J. Magn. Res.* 44:447–469.
27. Hagen, W. R., D. O. Hearshen, R. H. Sands, and W. R. Dunham. 1985. A statistical theory for powder EPR in distributed systems. *J. Magn. Res.* 61:220–232.
28. Pinkowitz, R. A., and P. Aisen. 1972. Zero-field splittings of iron complexes of transferrins. *J. Biol. Chem.* 247:7830–7834.
29. Gibson, J. F. 1978. Some recent EPR studies on metalloproteins. *J. Mol. Struct.* 45:139–157.
30. Aisen, P., A. Leibman, and J. Zweier. 1978. Stoichiometric and site characteristics of the binding of iron to human transferrin. *J. Biol. Chem.* 253:1930–1937.
31. Aasa, R. 1972. Re-interpretation of the electron paramagnetic resonance spectra of transferrins. *Biochem. Biophys. Res. Commun.* 49:806–812.
32. Princiotto, J. V., and E. J. Zapolski. 1975. Difference between the two iron-binding sites of transferrin. *Nature (Lond.).* 255:87–88.
33. Froncisz, W., and J. S. Hyde. 1982. The loop-gap resonator: a new microwave lumped circuit ESR sample structure. *J. Magn. Res.* 47:515–521.